EXPERIMENTAL STUDY OF EFFECTS OF FOREBODY GEOMETRY ON HIGH ANGLE OF ATTACK STATIC AND DYNAMIC STABILITY AND CONTROL

ICAS-86-5.4.1

Jay M. Brandon; Daniel G. Murri; and Luat T. Nguyen
NASA Langley Research Center
Mail Stop 355
Hampton, Virginia 23665-5225

Abstract

A series of low-speed wind tunnel tests on a generic airplane model with a cylindrical fuselage were made to investigate the effects of forebody shape and fineness ratio, and fuselage/wing proximity on static and dynamic lateral/directional stability. In addition, some preliminary testing to determine the effectiveness of deflectable forebody strakes for high angle of attack yaw control was conducted. During the stability investigation, 11 forebodies were tested including 3 different cross-sectional shapes with fineness ratios of 2, 3, and 4. In addition, the wing was tested at two longitudinal positions to provide a substantial variation in forebody/wing proximity. Conventional force tests were conducted to determine static stability characteristics, and single-degree-of-freedom free-to-roll tests were conducted to study the wing rock characteristics of the model with the various forebodies. Flow visualization data were obtained to aid in the analysis of the complex flow phenomena involved. The results show that the forebody cross-sectional shape and fineness ratio and forebody/wing proximity can strongly affect both static and dynamic (roll) stability at high angles of attack. These characteristics result from the impact of these factors on forebody vortex development, the behavior of the vortices in sideslip, and their interaction with the wing flow field. Preliminary results from the deflectable strake investigation indicated that forebody flow control using this concept can provide very large yaw control moments at stall and post-stall angles of attack.

Introduction

Numerous studies have shown that the forebody aerodynamics can dominate the stability characteristics of aircraft at high angles of attack (ref. 1-6). In addition it has been observed that some forebody geometries which provide favorable static stability characteristics can cause dynamic instabilities due to loss of yaw damping (ref. 7). More recently, studies have shown that forebody aerodynamics can also strongly affect dynamic roll stability (ref. 8 and 9). Loss of roll damping at high angles of attack can lead to wing rock which is an undesirable sustained oscillation, primarily in roll, that is exhibited by many modern aircraft. A research program is underway at the NASA Langley Research Center to provide a systematic low-speed wind-tunnel data base on the effects of forebody geometry on aircraft static and dynamic stability at high angles of attack. The primary goal of these studies is to advance understanding of the complex flow phenomena involved at high angle of attack flight conditions. Research is focusing on wind tunnel studies of a very simple generic airplane model with geometry flexibility, This geometric flexibility allows investigation of primary design factors including forebody cross-sectional shape and fineness ratio, wing planform and location, and empennage geometry. Results from the first series of tests of this model were reported in reference 9 and showed that forebody/wing flow coupling can dominate the static and dynamic stability near stall. To further explore this phenomenon, a current study is focused on the effects of forebody length and forebody/wing proximity. Forebody length was varied by testing specific forebody shapes over a range of fineness ratios while forebody/wing proximity was investigated by moving the wing longitudinally along the fuselage. This paper will review some of the results of these tests.

The potentially dominant influence of the forebody on high angle-of-attack stability suggests that proper control of the forebody flow could produce the desired levels of control forces and moments at high angle of attack where conventional controls are ineffective. For example, the conventional rudder generally loses effectiveness rapidly once it is immersed in the low-energy separated flow from the wing. A research program is being conducted at Langley to explore the concept of deflectable strakes intended to generate an intense vortex pair on a forebody of arbitrary shape. Manipulation of these vortices by deflecting the strakes would alter the symmetry of the overall forebody flow, thus producing the desired variable sideforces and yawing moments. Exploratory tests of this concept are being conducted using the same generic airplane model. This paper will highlight some of the preliminary results obtained to date in this ongoing program.

Symbols

b	wing span, ft
$\bar{c}$	mean aerodynamic chord length, ft
C_L	lift coefficient
C_ℓ	rolling moment coefficient
$\hat{C}_\ell$	estimated rolling-moment coefficient
C_{ℓ_β}	lateral-stability derivative, $\frac{\partial C_\ell}{\partial \beta}$, deg^{-1}
C_{ℓ_p}	roll-damping coefficient, $\frac{\partial C_\ell}{\partial (\frac{pb}{2V})}$, rad^{-1}
C_m	pitching-moment coefficient
C_n	yawing-moment coefficient
C_{n_β}	directional-stability derivative, $\frac{\partial C_n}{\partial \beta}$, deg^{-1}
I_x	roll moment of inertia, slug-ft
L	left side
p	roll rate, rad/sec
q	dynamic pressure, psf
R	right side
S	wing area, ft^2
V	free stream velocity, ft/sec
α	angle of attack, deg
α_o	angle of attack at $\phi = 0°$, deg
β	angle of sideslip, deg
δ_r	rudder deflection angle, deg
δ_s	forebody strake deflection angle, deg

effect is much stronger than the effect due to forebody fineness ratio. For example, at $\alpha = 30^0$ moving the wing forward results in a variation from highly stable to moderately unstable regardless of forebody length.

Figure 19 summarizes the effect of forebody length and wing location on C_{ℓ_β} for the vertical ellipse forebody configurations. For a given wing position, it is seen that the variations in fineness ratio have very small effects on the static lateral stability. On the other hand, forebody-wing proximity strongly influences the values of C_{ℓ_β} for angles of attack between 15° and 35°. The results show that moving the wing closer to the forebody significantly enhances lateral stability, which is exactly opposite the effect observed for the horizontal ellipse configurations.

Figure 20 presents photographs of smoke flow visualization taken at $\alpha_o = 35°$ with the model rolled approximately 10 degrees right wing down. The wing was in the forward location and the model was fitted with fineness ratio 3 noses. Smoke was injected at the wing root on the leeward side. With the horizontal ellipse configuration, the smoke flows show that the leeward forebody vortex passed over the inboard section of the left wing augmenting lift on that wing. This leeward wing lift contributed to the unstable lateral stability exhibited by this configuration. In contrast, the vertical ellipse configuration developed a leeward vortex which passed over the fuselage and was situated over the windward wing root. As a result a lift increment was produced on the windward wing which provided lateral stability.

Dynamic Roll Stability

Effect of Forebody Cross-Sectional Shape

Free-to-roll results for the configuration showed that wing rock oscillations of varying amplitudes were exhibited by most of the configurations between 25° to 40° angle of attack. In this angle of attack range, the model began a roll oscillation without any external disturbance beyond the inherent turbulence of the tunnel. This characteristic is illustrated in figure 21 which presents a time history of the roll angle of the model with the horizontal ellipse nose with fineness ratio of 3. The model was released from an initial stationary position at $\alpha_o = 35°$ and $\phi = -6°$. It is seen that a large amplitude wing rock motion built up rapidly over two to three oscillation cycles and that the "steady state" oscillations were somewhat irregular with significant amplitude variations from cycle to cycle.

A summary of the free-to-roll results for the various nose shapes for a fineness ratio of 3 with the nominal wing position is presented in figure 22 in terms of observed oscillation amplitude versus angle of attack. These results indicate a significant effect of forebody cross-sectional shape on wing rock characteristics. The vertical ellipse nose shape was the most resistant to wing rock, exhibiting only small amplitude oscillations between 25 and 30 degrees angle of attack. The horizontal ellipse forebody produced the largest amplitude of wing rock with amplitudes reaching $\Delta\phi = 40°$. Correlating these results to the static lateral stability data shown in figure 13, a trend is observed that the nose shapes which provide the highest levels of static stability also tend to cause the highest amplitude of wing rock and vice versa.

Effect of Fineness Ratio and Forebody/Wing Proximity

The effect of forebody length on wing rock amplitude is illustrated in figure 23. Shown are data obtained at $\alpha_o = 35°$ for the various forebody shapes at fineness ratios of 2, 3, and 4. The results indicate that forebody length can significantly influence wing rock amplitude. However, attempts at correlating these data with the static stability data did not define any consistent trends.

Wing rock data for the wing in the forward position are summarized in figure 24. These results should be compared to those of figure 22 to assess the impact of forebody/wing proximity. It is seen that moving the wing forward dramatically altered the wing rock characteristics. For example, with the wing in the nominal position, the horizontal ellipse configuration exhibited large amplitude wing rock above 25 degrees angle of attack. On the other hand, the vertical ellipse configuration showed only small amplitude oscillations for angles of attack up to 30°. These characteristics are completely reversed with the wing in the forward position. The horizontal ellipse configuration became extremely resistant to wing rock, whereas the vertical ellipse configuration exhibited very large amplitude wing rock between 20° and 40° angle of attack. It is interesting to correlate these results to the static lateral stability discussed earlier. A clear trend is apparent that when moving the wing forward (thus bringing it closer to the forebody) reduced static lateral stability, it also reduced wing rock amplitude and vice versa. This result is illustrated in figure 25 which presents a cross plot of C_{ℓ_β} and $\Delta\phi$ for the horizontal and vertical ellipse configurations with the two wing positions at $\alpha_o = 30°$. The trend indicated in the plot also reinforces the observation stated earlier that configurations having the highest levels of static stability also tend to exhibit the largest amplitude of wing rock; whereas configurations that have no static stability are wing rock resistant.

Aerodynamic Moments During Wing Rock

As discussed earlier, estimates of the aerodynamic rolling moment coefficient during wing rock were made by differentiating the roll displacement signal. These data were used to examine the time varying loads that drove the limit-cycle oscillations. As an example, results will be discussed for a configuration incorporating the fineness ratio 4 vertical ellipse nose with the wing in the forward position. This configuration was found to exhibit large amplitude wing rock, as illustrated in figure 26 which shows a wing rock build-up to the limit cycle starting from $\alpha_o = 35°$. To aid in the analysis of these motions, static data were measured at the combinations of α and β corresponding to the roll angles encountered during the free-to-roll tests. The rolling moment data are shown in figure 27 as a plot of C_ℓ versus ϕ. The results indicate high levels of stability (negative slope) for roll angles up to about ±40°. It is interesting to note that the observed wing rock amplitude at this condition was approximately 45°. Figure 28 presents estimates of the rolling moment

coefficients obtained from the free-to-roll data plotted versus roll angle. Results are shown for three ranges of reduced roll rates: $\frac{pb}{2V} \approx 0$, and $\frac{pb}{2V} \approx \pm.026$. Comparison of the $\frac{pb}{2V} \approx 0$ data to the static wind tunnel data shown in figure 27 indicate fairly good agreement which provides a check of the validity of the estimated coefficients. Comparison of the $\frac{pb}{2V} \approx \pm.026$ and $\frac{pb}{2V} \approx 0$ data indicates that for the smaller roll angles ($\phi < 20°$), the dynamic rolling moment differs significantly from the static values. For positive roll rates the dynamic values are consistently higher than static and conversely, at negative roll rate the dynamic values are more negative than the static values indicating unstable roll damping. At larger roll angles, the differences between static and dynamic rolling moment become less distinct. This behavior is similar to that postulated to cause the wing rock exhibited by slender delta wings as discussed in reference 12.

To further assess the variation of roll damping, figure 29 shows estimated rolling moment plotted versus reduced roll rate. The results were obtained by analyzing data at $\phi = 0°$ over a large number of oscillation cycles. The plot indicates that at low rates, the roll damping is unstable as shown previously in figure 28. Calculation of the slope gives a value of the roll damping parameter, C_{ℓ_p}, of 0.18. Additionally, however, the data show that at higher roll rates the damping becomes stable. The characteristic of unstable roll damping at small roll rates combined with stable damping at higher rates would promote the limit-cycle type wing rock observed in the free-to-roll tests.

Forebody Flow Control

The dominant influence of the forebody vortex flowfield on the stability characteristics at high angles of attack suggests the possibility of utilizing the forebody for control in the angle of attack range where conventional aerodynamic controls become ineffective. Typical aircraft rapidly lose rudder yaw control as wing stall develops and the vertical tail(s) becomes immersed in the low-energy, separated wake from the wing. Since the forebody cross-sectional shape has been shown to be a dominant contributor to high angle of attack characteristics, the current study focused on a concept to provide an alternate means of yaw control using deflectable forebody strakes to change the effective cross sectional shape, thereby producing a controlled vortex asymmetry and thus a variable yawing moment. For the initial tests, it was desired to keep the forebody shape as simple as possible so that the effect of the strakes would be easier to analyze. As a result, a conical shaped nose with a fineness ratio of 3 was used. Thin tapered aluminum strakes (chord = .3 local forebody radius) were tested at a variety of radial locations on the forebody and at a variety of strake deflections (see fig. 5).

Initial studies were made to evaluate the potential to develop a vortex asymmetry by testing the body alone model (wing and tails off) with a single strake mounted on the left side of the forebody. Figure 30 presents a comparison of the yawing moment generated by a single strake at three radial locations and includes sketches of the flow mechanism based on flow visualization tests. At radial locations (ϕ_s) less than 80 degrees, the largest yawing moments were obtained with $\phi_s = 60°$. In this region of ϕ_s, the yawing moment produced was generally negative suggesting that the suction induced by the strake vortex was greater than the suction on the opposite side of the forebody. With $\phi_s = 60°$, the data show yawing moment developing at $\alpha = 20°$, increasing to a maximum at $\alpha = 45°$, and then decreasing to a near constant value between 60° and 80° angle of attack. The data for $\phi_s = 80°$ indicate less of an asymmetry than for $\phi_s = 60°$, with yawing moment initially generated in the negative direction and then reversing to a positive direction above $\alpha = 55°$. As ϕ_s increases above 80°, the yawing moment is generally nose right indicating that the prevailing suction occurs on the "clean" side of the forebody. For these cases, the largest moments were measured for $\phi_s = 105°$. The data for this configuration show yawing moment developing at about $\alpha = 20°$, increasing to a maximum at $\alpha = 50°$, and decreasing to a near constant value between $\alpha = 60°$ and 80°.

Once the radial locations favorable to generating a yawing moment with a single strake were determined, tests were conducted to evaluate the effectiveness of varying the strake deflection angle at fixed values of ϕ_s. At $\phi_s = 60°$, data indicated that both up and down strake deflections were effective in varying the yawing moment by displacing the strake vortex. This result suggests that a pair of strakes positioned symmetrically at $\phi_s = 60°$ on either side of the forebody and deflected in an anti-symmetric mode could produce useful levels of yaw control. Results obtained for the body alone model are presented in figure 31 which shows control effectiveness for anti-symmetric strake deflection, although the angle of attack of initial effectiveness is delayed to about $\alpha = 40°$. At the $\phi_s = 105°$ location, data indicated that the strake-up deflections were more effective in varying yawing moment than strake-down deflections. The amount of yawing moment generated by the forebody strake was found to be effectively controlled by the variation of strake deflection angle. Figure 32 shows the effect of strake deflection on yawing moment for the strake at $\phi_s = 105°$. These results suggest that strakes on each side of the forebody could be deployed singly to produce the direction and level of yaw control desired.

For the complete configuration (with wing and horizontal and vertical tails), a comparison of the control power available with the forebody strake concept with that of a conventional rudder is presented in figure 33. The data show that while the conventional rudder begins to lose yaw control effectiveness above $\alpha = 10°$, the forebody strake configuration increases in effectiveness and provides very large increments in yaw control to much higher angles of attack. For the $\phi_s = 105°$ case, figure 34 presents the variation of yaw control power with strake deflection along with the associated effects on the rolling and pitching moments. The yawing moment data of figure 34 show that below $\alpha = 30°$, the level of yaw control was insensitive to strake deflection. Above $\alpha = 30°$, however, the data indicate a controllable variation of yawing moment with strake deflection. The other two plots show that the strake control coupling in roll is

minimal for all strake deflections, and that coupling in pitch is small except for $\delta_s = 0°$. The incremental nose-up moment associated with $\delta_s = 0°$ is probably the result of the significant increase in effective forebody planform area caused by the strake. It is noted, however, that large yaw control increments are still available even if the strake deflection is limited to 30°, which would eliminate any significant coupling in pitch.

An additional characteristic of the deflectable strake concept which must be evaluated is the effectiveness of the control at sideslip. Shown in figure 35 is the yaw control effectiveness of the $\phi_s = 105°$ configuration at 50 degrees angle of attack over a sideslip range of ±30°. The data indicate that, despite the significant variation with β, this strake configuration is effective over a wide range of sideslip from $\beta = -20°$ to 15°.

It is interesting to note some of the differences between the deflectable strake concept and a previously studied concept, forebody blowing, presented in reference 11. Although both methods produce large yawing-moment increments at high angles of attack, the mechanisms which provide the control are very different. At high angle of attack, forebodies which generate strong, closely spaced vortices develop flow asymmetries resulting in one vortex further above the forebody surface than the other. Forebody blowing is used to control vortex asymmetry and thereby yawing-moment produced by the forebody. This method was found to be limited in sideslip due to the strong effect of sideslip on vortex asymmetry. The current method acts in a very different manner. The strake deflection alters the effective cross-sectional shape of the forebody and thereby the forebody vortex pattern. Variation of the nose geometry in this fashion was found to give fairly linear control moments with strake deflection angle at high angles of attack, and also maintained effectiveness at sideslip.

Although these preliminary results are promising, much additional research is required to further understand the flow mechanisms involved (particularly the effects of Reynolds number), to study application to other forebody shapes, to assess the effect of the strakes on dynamic stability, and to investigate any lag effects associated with the deflection of the strakes which could impact the operational usage of the strakes as a control device.

Concluding Remarks

This paper has summarized recent research at the NASA Langley Research Center on the effects of forebody flows on static and dynamic stability at low-speed, high angle-of-attack conditions and on manipulation of these flows to produce large yaw control moments. The results of the stability tests show that forebody cross-sectional shape and fineness ratio, and the proximity of the wing to the forebody can strongly affect static and dynamic stability in the angle of attack range around stall. Cross-sectional shape and fineness ratio influence the development and strength of the forebody vortices, their behavior in sideslip, and their interaction with the wing flow field. Forebody/wing proximity directly affects the coupling of the two flow fields and as a result can profoundly influence static and dynamic roll stability at high angles of attack. The combination of these factors produced static lateral/directional stability characteristics that ranged from highly stable to highly unstable and configurations that were well damped in roll to those that exhibited very large amplitude wing rock. A general trend was observed whereby configurations that had the highest levels of static lateral stability also tended to exhibit the largest amplitude wing rock, whereas configurations that were statically unstable were very resistant to wing rock. Follow-on tests are planned which will examine other configuration design factors including wing planform and placement and empennage geometry. In addition, more detailed flow visualization and measurements will be made to aid in analysis of the very complex flow mechanisms involved, particlarly during wing rock. It is recognized that this set of data is being generated in wind tunnel tests conducted at very low Reynolds number and that forebody separation phenomena are known to be Reynolds number sensitive. High Reynolds number data will ultimately also have to be obtained in order to assess viscous effects and to allow confident application of the results to full scale conditions.

The preliminary results for the forebody strakes are very promising in that the deflectable strakes were able to generate yaw control moments at stall and post stall angles of attack that are much larger than those available from a conventional rudder. However, much additional testing involving detailed flow visualization and pressure measurements is needed to further understand the dominant flow mechanisms that provide these characteristics. Upcoming tests will also investigate the effects of strake size and location, and the application of this concept to other forebody shapes. The possibility of using these devices to alter the forebody/wing flow field interaction and thereby controlling wing rock will also be investigated.

References

1. Grafton, S. B.; Chambers, J. R.; and Coe, P. L., Jr.: Wind Tunnel Free-Flight Investigation of a Model of a Spin Resistant Fighter Configuration. NASA TN D-7716, June 1974.

2. Skow, A. M.; and Erickson, G. E.: Modern Fighter Aircraft Design for High Angle-of-Attack Maneuvering. AGARD Lecture Series No. 121 on High Angle-of-Attack Aerodynamics, March 1982.

3. Carr, Peter; and Gilbert, William: Effects of Fuselage Forebody Geometry on Low-Speed Lateral-Directional Characteristics of a Twin-Tail Fighter Model at High Angles of Attack. NASA TP 1592, 1979.

4. Klein, John; Walch, Kenneth; and Hahne, David: Airframe Component Effects on the Aerodynamic Stability and Control Characteristics of a Supersonic Cruise Fighter Aircraft at High Angles of Attack. AIAA Paper No. 84-2110, August 1984.

5. Erickson, Gary; and Gilbert, William: Experimental Investigation of Forebody and Wing Leading-Edge Vortex Interactions at High Angles of Attack. AGARD Conference Proceedings No. 342, March, 1984.

6. Erickson, Gary; and Brandon, Jay: Low-Speed Experimental Study of the Vortex Flow Effects of a Fighter Forebody Having Unconventional Cross-Section. AIAA Paper No. 85-1798-CP, August 1985.

7. Murri, D. G.; Nguyen, L. T.; and Grafton, S. B.: Wind Tunnel Free-Flight Investigation of a Model of a Forward-Swept-Wing Fighter Configuration. NASA TP 2230, 1984.

8. Nguyen, L. T.; Whipple, R. D.; and Brandon, J. M.: Recent Experiences of Unsteady Aerodynamic Effects on Aircraft Flight Dynamics at High Angle of Attack. AGARD Conference Proceedings No. 386, Paper No. 28, 1985.

9. Brandon, J. M.; and Nguyen, L. T.: Experimental Study of Effects of Forebody Geometry on High Angle of Attack Static and Dynamic Stability. AIAA Paper No. 86-0331, January 1986.

10. Rao, D. M.; and Murri, D. G.: Exploratory Investigation of Deflectable Forebody Strakes for High Angle-of-Attack Yaw Control. AIAA Paper No. 86-0333, January 1986.

11. Skow, A. M.; Moore, W. A.; and Lorincz, D. J.: Forebody Vortex Blowing -- A Novel Control Concept to Enhance Departure/Spin Recovery Characteristics of Fighter and Trainer Aircraft. AGARD Conference Proceedings No. 262, Paper No. 24, 1979.

12. Nguyen, L. T.; Yip, L. P.; and Chambers, J. R.: Self Induced Wing Rock of Slender Delta Wings. AIAA Paper No. 81-1883, August 1981.

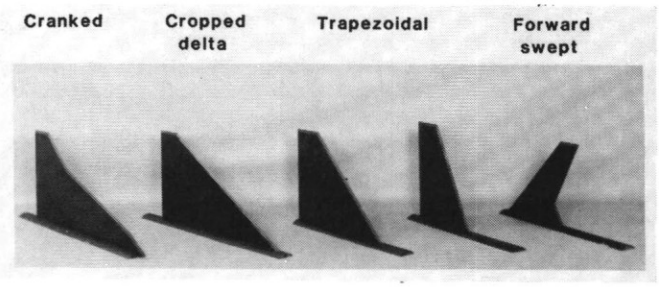

Figure 1 - Wing shapes for generic airplane model.

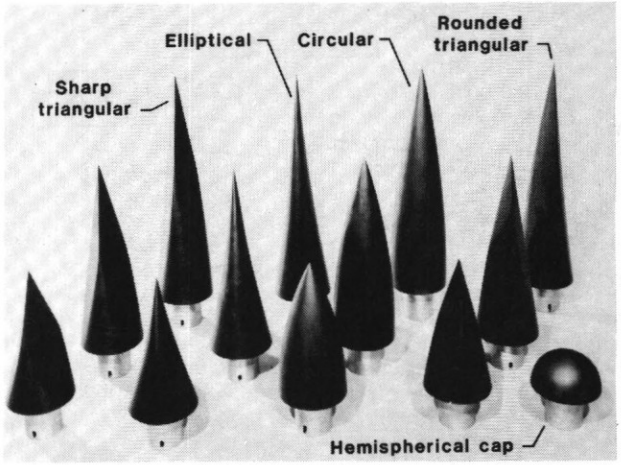

Figure 2 - Forebodies available for generic airplane model.

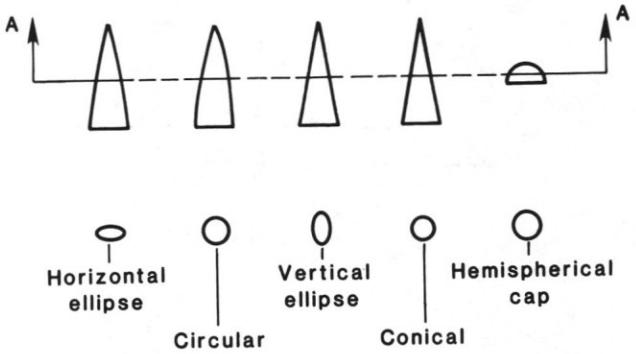

Figure 3 - Forebody cross-sectional shapes tested.

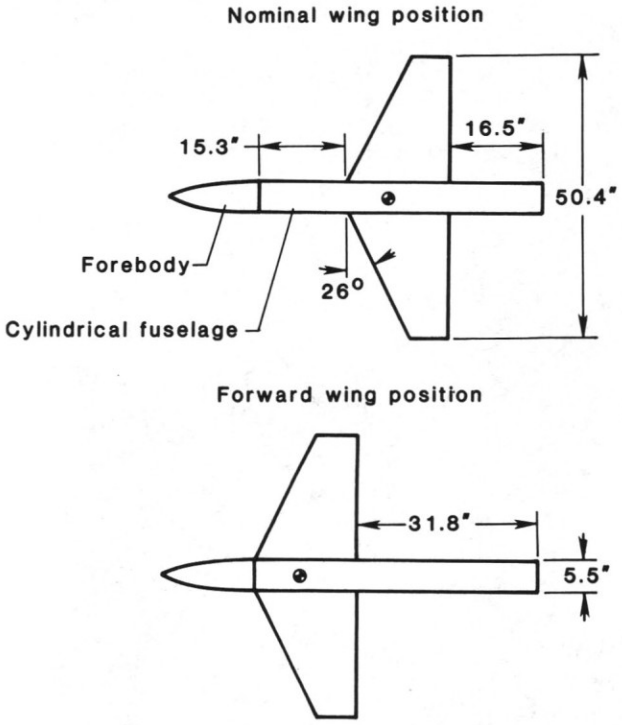

Figure 4 - Wing positions tested.

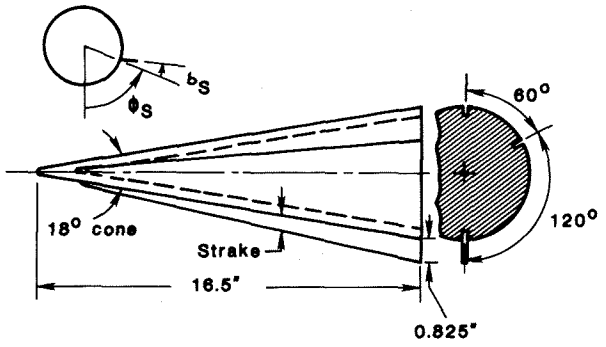

Figure 5 - Conical forebody tested with forebody strakes.

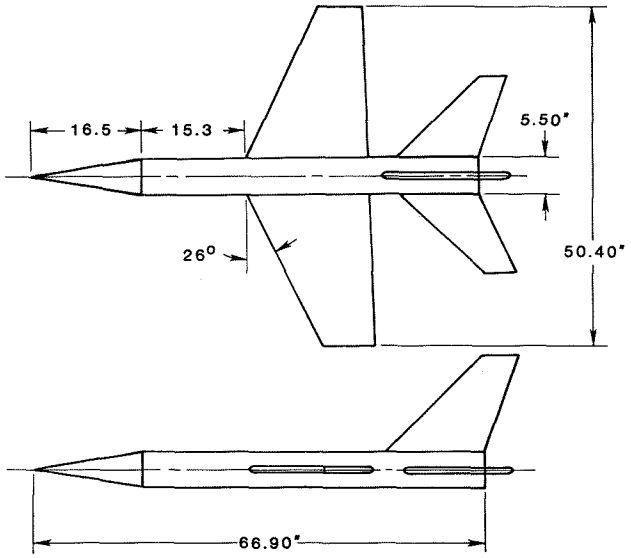

Figure 6 - Drawing of model configuration for forebody strake control study.

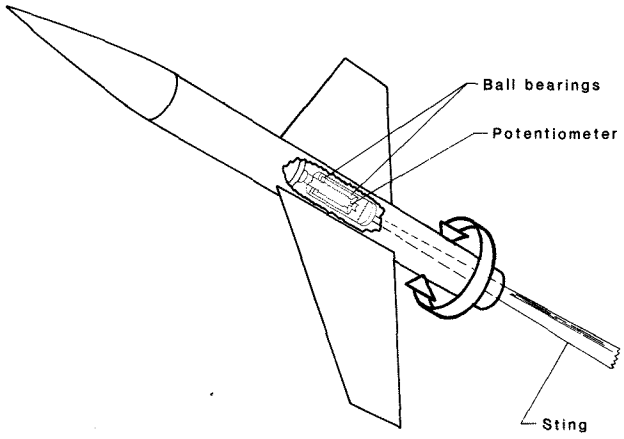

Figure 7 - Free-to-roll test apparatus.

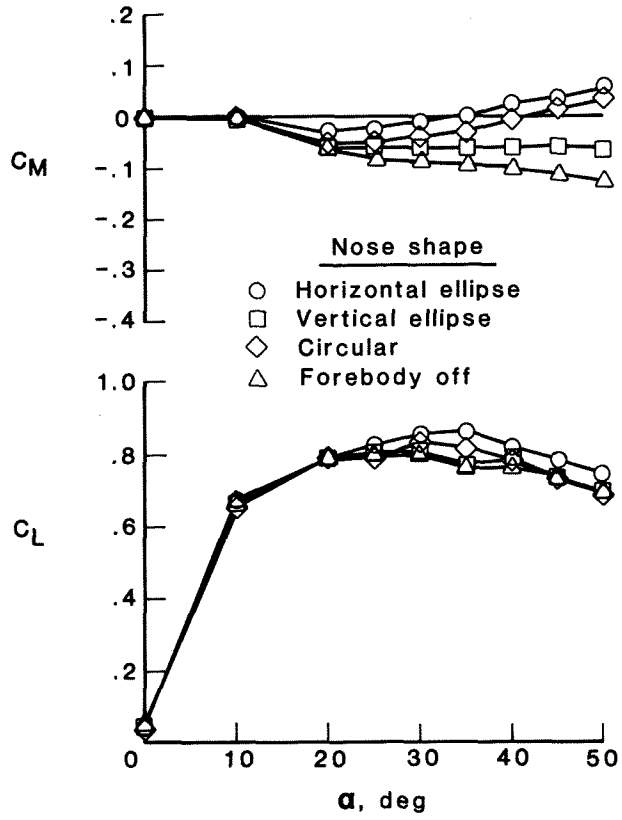

Figure 8 - Effect of forebody cross-sectional shape on longitudinal stability. Fineness ratio = 3. Nominal wing position.

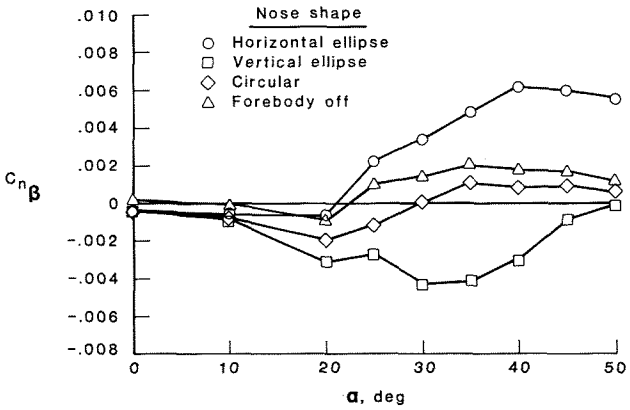

Figure 9 - Effect of forebody cross-sectional shape on directional stability. Fineness ratio = 3. Nominal wing position.

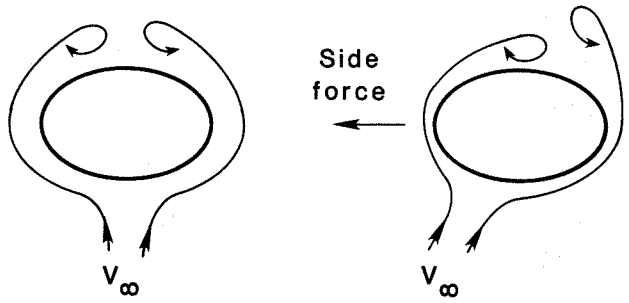

Figure 10 - Flow pattern above horizontal ellipse forebody. $\alpha = 30^o$.

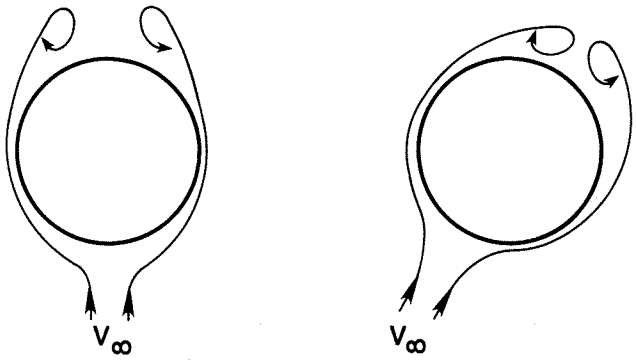

Figure 11 - Flow pattern above circular forebody. $\alpha = 30^o$.

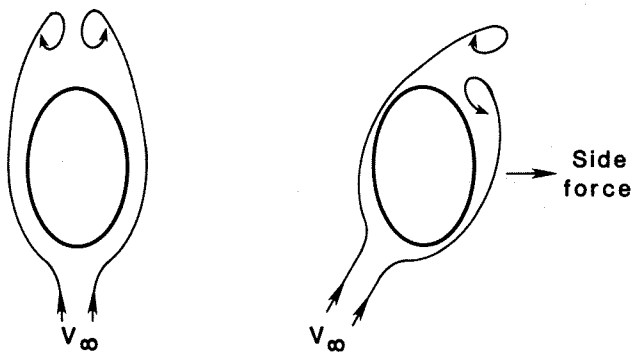

Figure 12 - Flow pattern above vertical ellipse forebody. $\alpha = 30^o$.

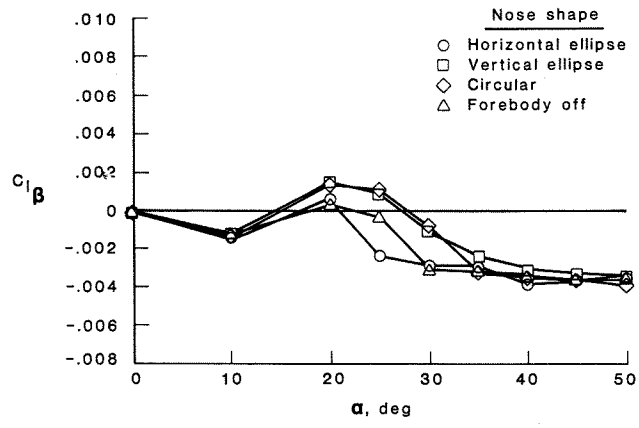

Figure 13 - Effect of forebody cross-sectional shape on lateral stability. Fineness ratio = 3. Nominal wing position.

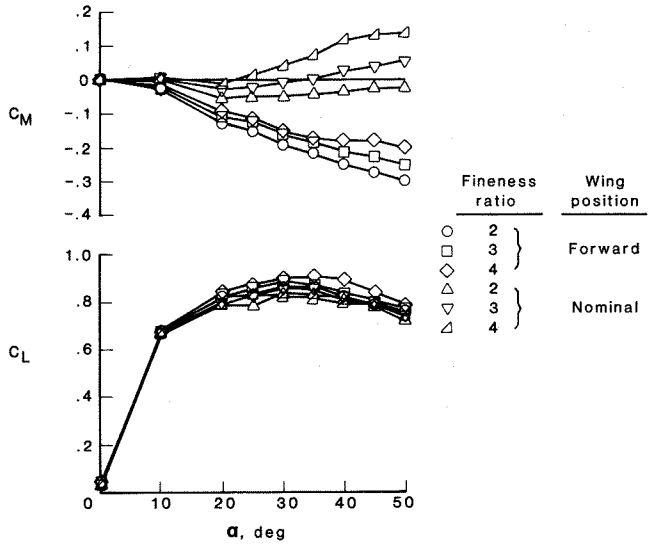

Figure 14 - Effect of fineness ratio and wing proximity on longitudinal stability. Horizontal ellipse forebody.

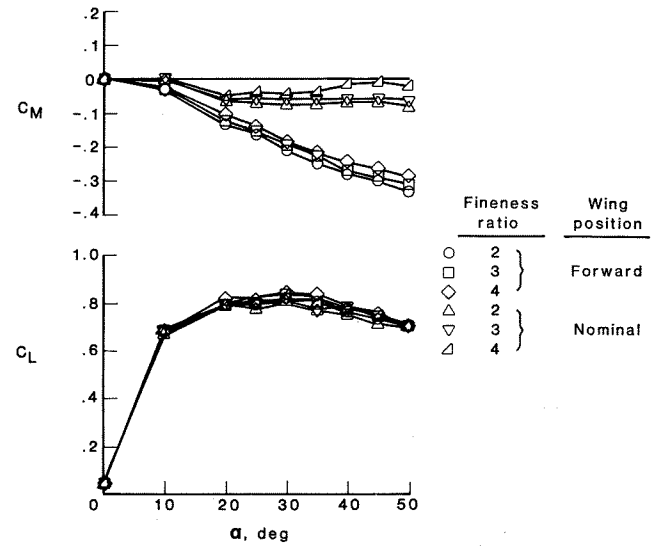

Figure 15 - Effect of fineness ratio and wing proximity on longitudinal stability. Vertical ellipse forebody.

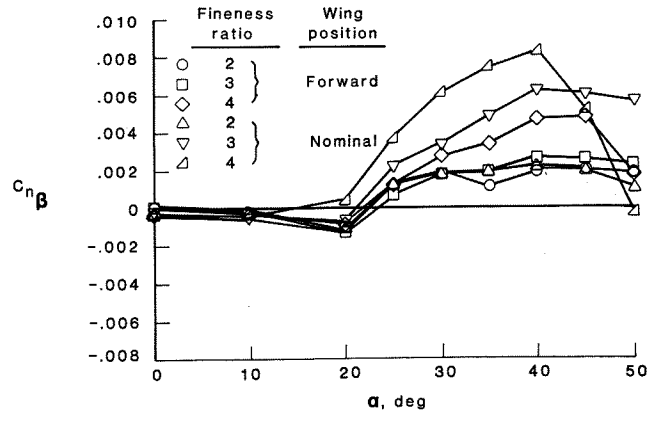

Figure 16 - Effect of fineness ratio and wing proximity on directional stability. Horizontal ellipse forebody.

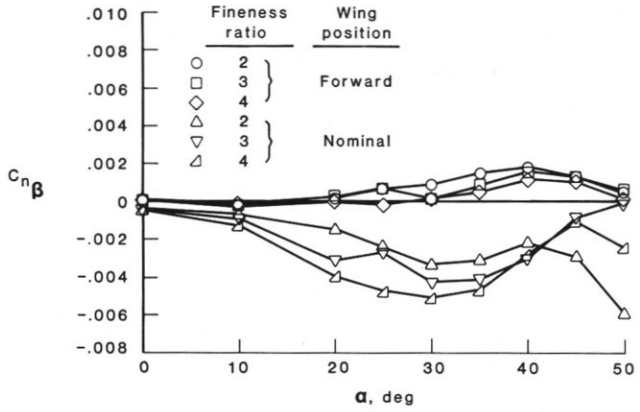

Figure 17 - Effect of fineness ratio and wing proximity on directional stability. Vertical ellipse forebody.

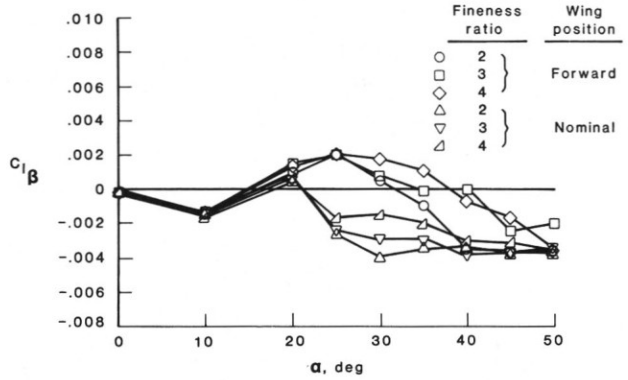

Figure 18 - Effect of fineness ratio and wing proximity on lateral stability. Horizontal ellipse forebody.

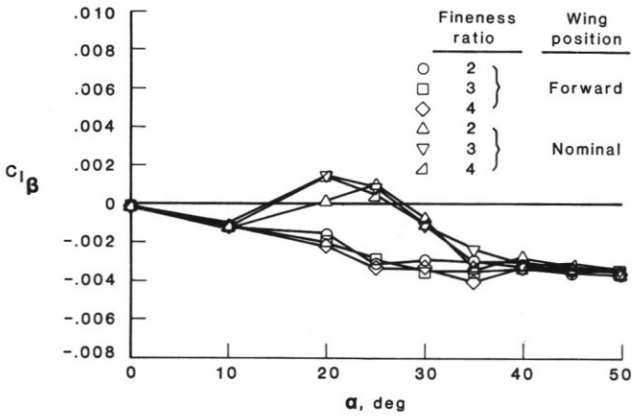

Figure 19 - Effect of fineness ratio and wing proximity on lateral stability. Vertical ellipse forebody.

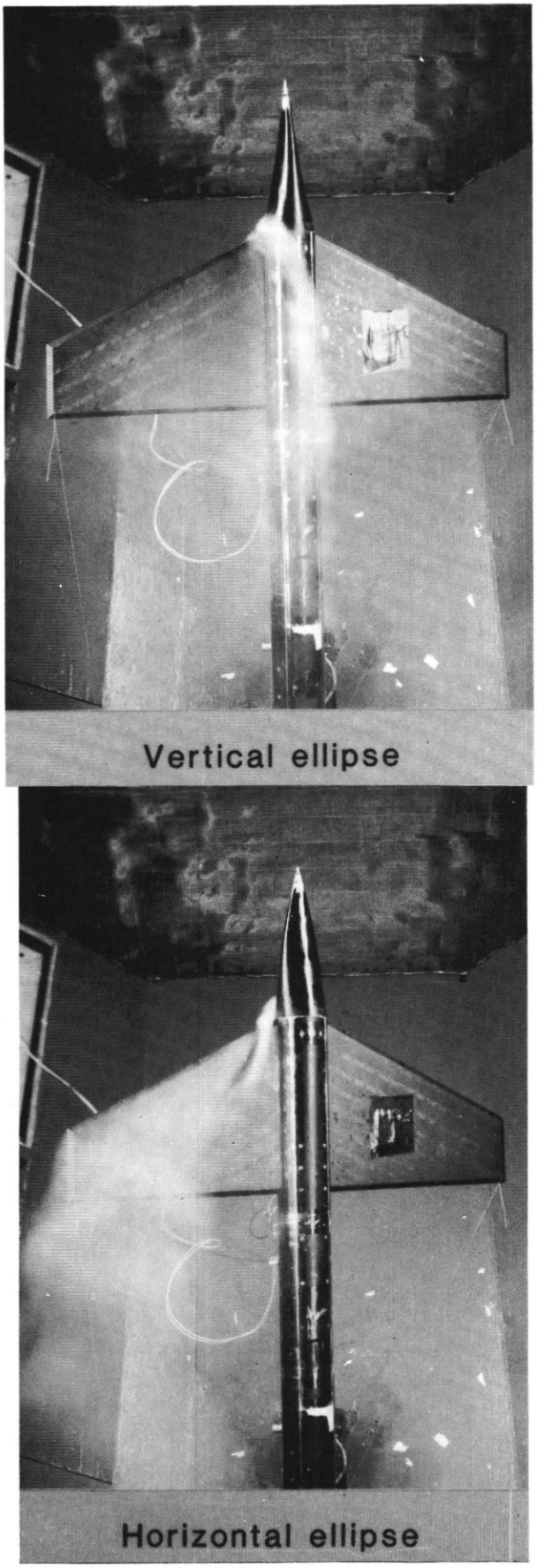

Figure 20 - Flow visualization over leeward wing. $\alpha_o = 35^o$, $\phi = 10^o$. Forebody fineness ratio = 3.

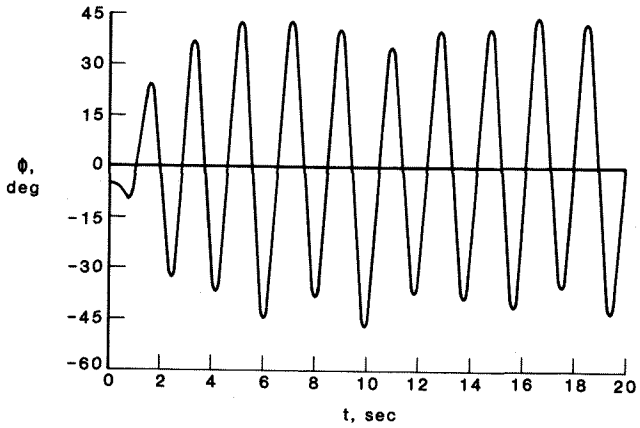

Figure 21 - Time history of wing rock build-up. Horizontal ellipse forebody. Fineness ratio = 3. α_o = 35°. Nominal wing position.

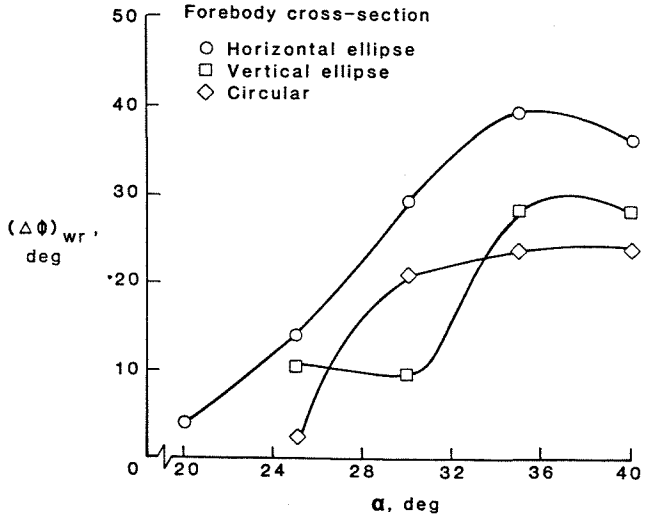

Figure 22 - Effect of forebody cross-section on wing rock amplitude. Fineness ratio = 3. Nominal wing position.

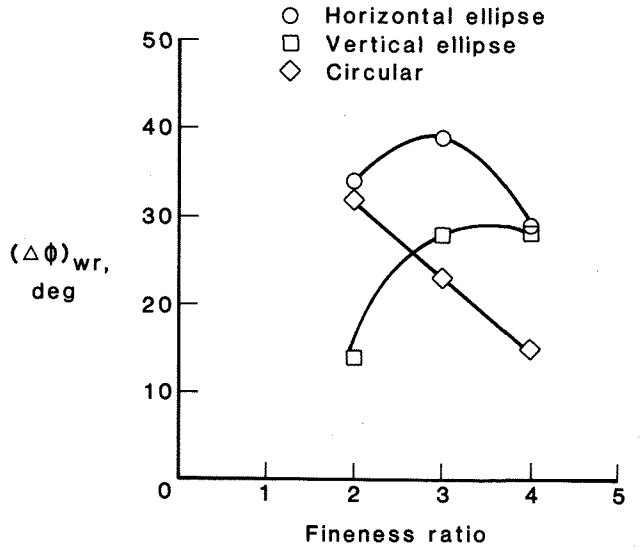

Figure 23 - Effect of forebody fineness ratio on wing rock amplitude. Nominal wing position. α_o = 35°.

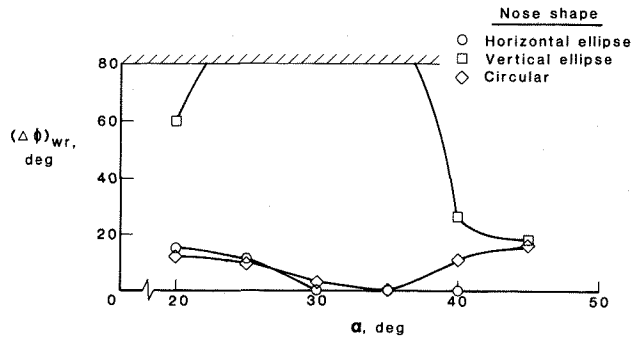

Figure 24 - Effect of forebody cross-section on wing rock amplitude. Fineness ratio = 3. Forward wing position.

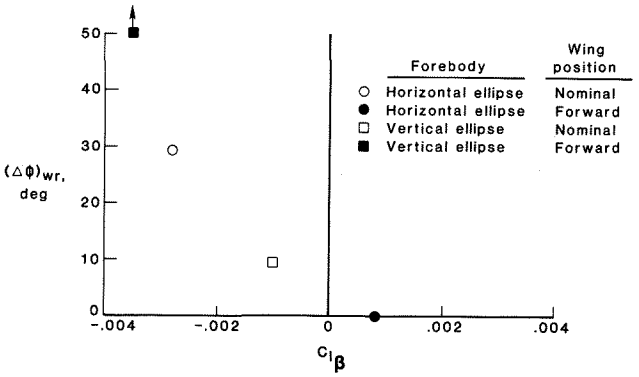

Figure 25 - Comparison of wing rock tendencies with static lateral stability. α_o = 30°. Forebody fineness ratio = 3.

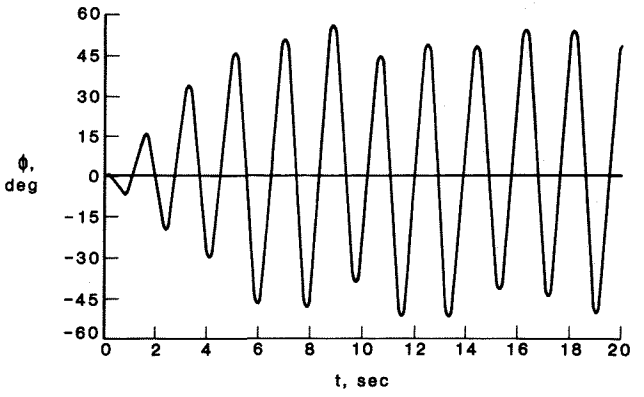

Figure 26 - Time history of wing rock build-up. Vertical ellipse forebody, Fineness ratio = 4. α_o = 35°. Forward wing position.

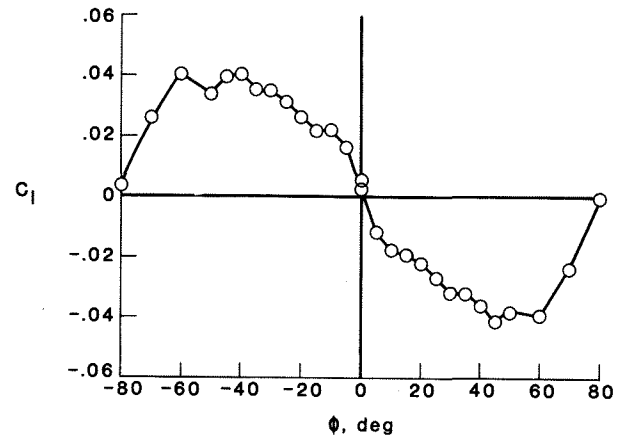

Figure 27 - Static rolling moment coefficient at roll angle. α_o = 35°. Vertical ellipse forebody, fineness ratio = 4. Forward wing position.

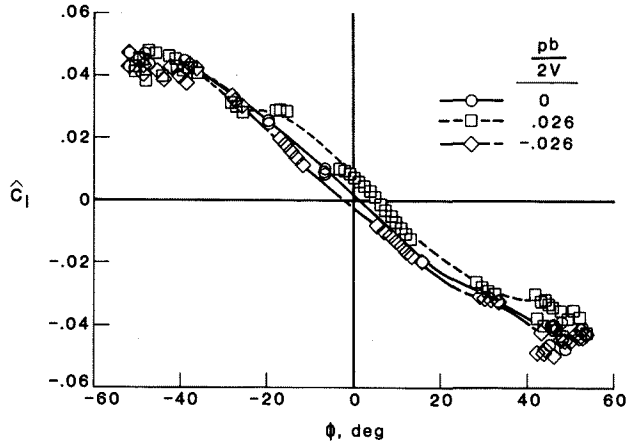

Figure 28 - Rolling moment coefficient during wing rock. Vertical ellipse forebody, fineness ratio = 4. α_o = 35°. Forward wing position.

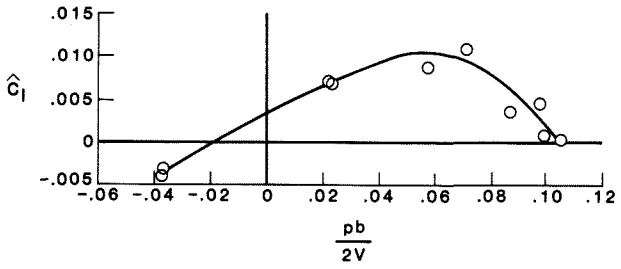

Figure 29 - Effect of roll rate on rolling moment during wing rock. ϕ = 0°. Vertical ellipse forebody, fineness ratio = 4. Forward wing position.

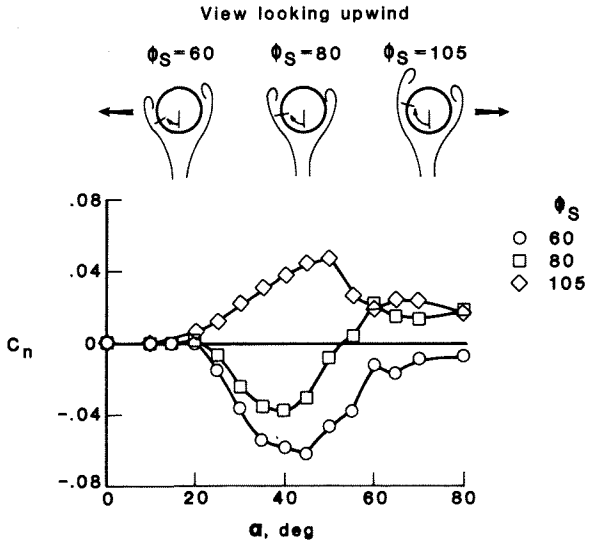

Figure 30 - Effect of strake position on yawing moment. Body alone.

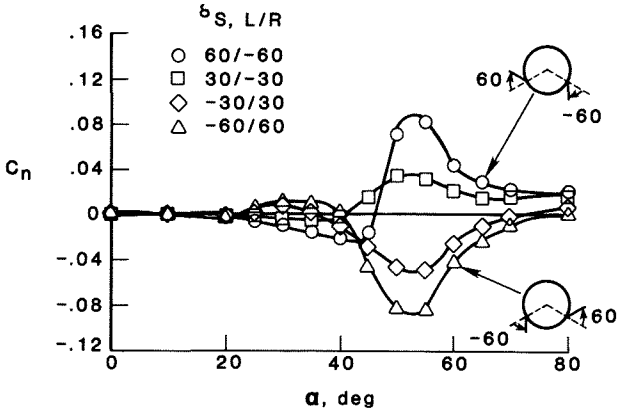

Figure 31 - Effect of anti-symmetric strake deflection on yawing moment. Body alone. ϕ_s = 60°.

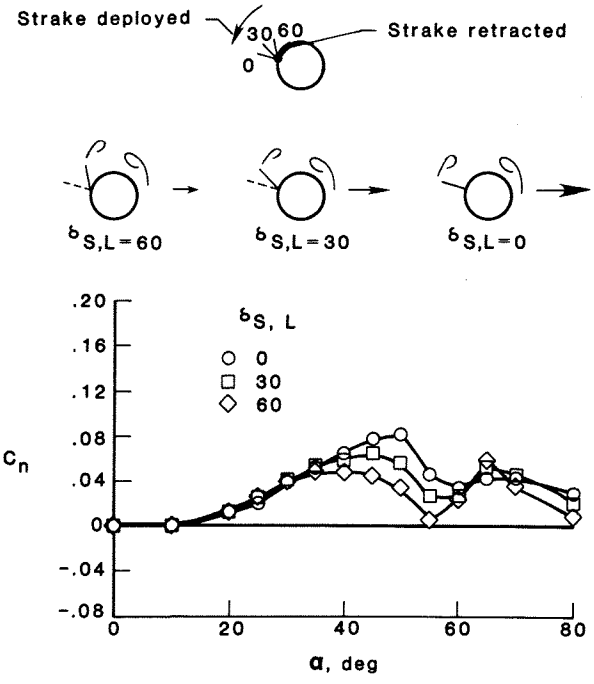

Figure 32 - Effect of strake deflection angle on yawing moment. Body alone. ϕ_s = 105°.

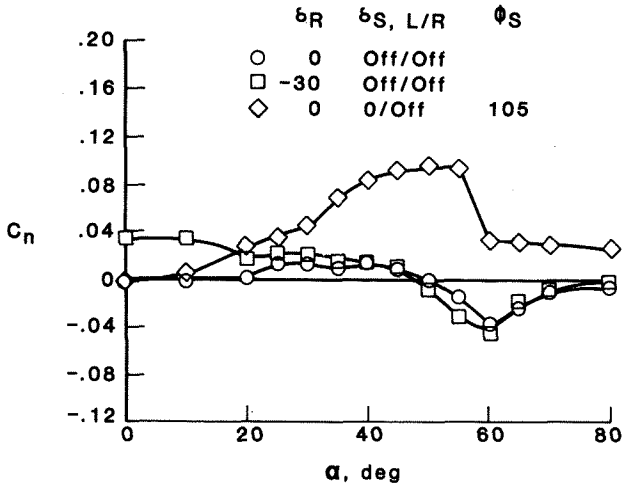

Figure 33 - Comparison of rudder and forebody strake control effectiveness for yaw control. Body, wing, and tails.

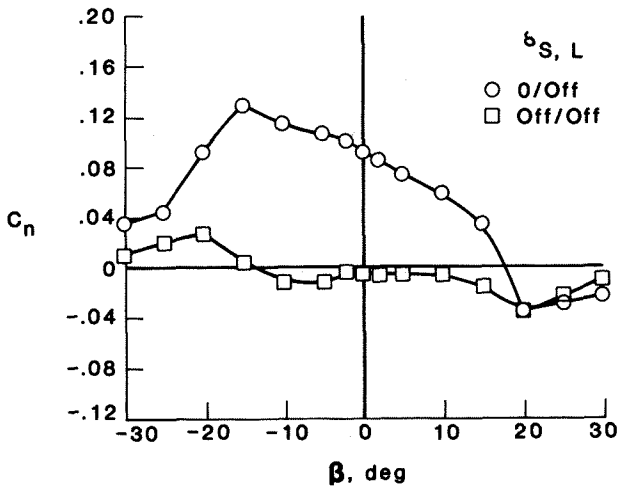

Figure 35 - Strake effectiveness in sideslip. Body, wing, and tails. $\alpha = 50^{o}$. $\phi_s = 105^{o}$.

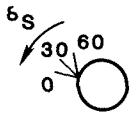

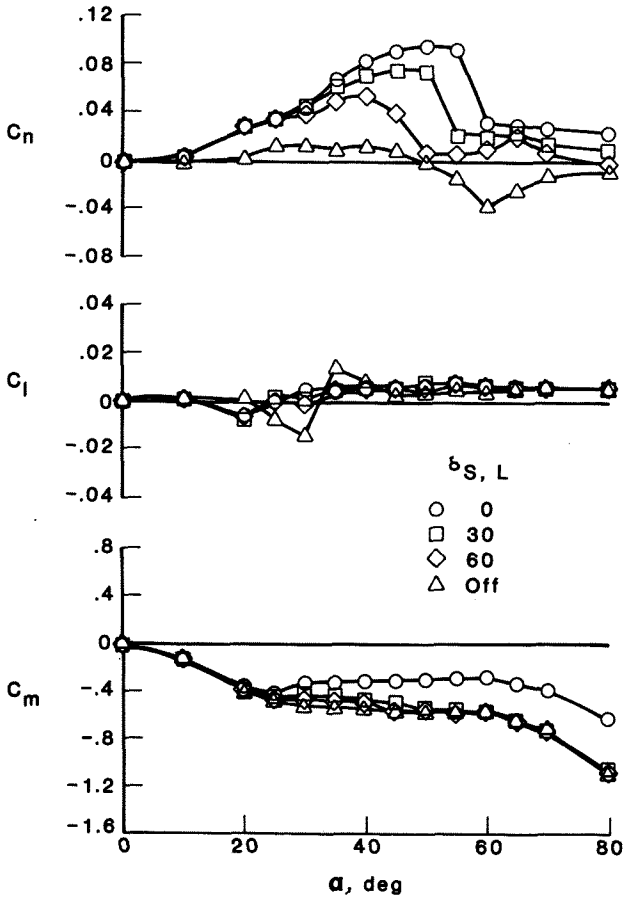

Figure 34 - Effect of strake deflection angle. Body, wing, and tails. $\phi_s = 105^{o}$.